



## Discovery of the EL-0052 as a potential anesthetic drug

Jun-hao Jiang<sup>a,1</sup>, Xiang-qing Xu<sup>b,1</sup>, Wen-gao Jiang<sup>a</sup>, Tao Wang<sup>c</sup>, Xin Liu<sup>a,c</sup>, Ling-guo Zeng<sup>c</sup>, Jian Liao<sup>c</sup>, Jing-ya Xiu<sup>c</sup>, Yi Shen<sup>c</sup>, Ping Deng<sup>a,\*</sup>, Qin-geng Li<sup>a,\*</sup>

<sup>a</sup> College of Pharmacy, Chongqing Medical University, Chongqing 400016, China

<sup>b</sup> Nhw Institute of Pharmaceutical Research, Jiangsu Nhw Pharmaceutical Corporation Ltd., Xuzhou 221009, China

<sup>c</sup> Jiangsu Nhw-Luokang Pharmaceutical Research And Development Corporation Ltd., Chongqing 404100, China



### ARTICLE INFO

#### Article history:

Received 18 November 2020

Received in revised form 3 January 2021

Accepted 5 January 2021

Available online 8 January 2021

#### Keywords:

Etomidate

Anesthetic

GABA<sub>A</sub>R

CYP11B

Adrenocortical suppression

Molecular docking

### ABSTRACT

As a  $\gamma$ -aminobutyric acid A receptor (GABA<sub>A</sub>R) inhibitor, etomidate fulfills several characteristics of an ideal anesthetic agent, such as rapid onset with rapid clearance and high potency, along with cardiovascular stability. Unfortunately, etomidate has been reported to inhibit CYP11B1 at hypnotic doses, which is associated with a marked increase in patient deaths due to this unexpected off-target effect. In this study, molecular docking was used to simulate the binding mode of etomidate with GABA<sub>A</sub>R and CYP11B1. Based on the in-depth analysis of the binding mode, strong electron-withdrawing group on the C4 position of the imidazole ring was introduced to reduce the charge density of the nitrogen, which is beneficial in reducing the coordination bond between the imidazole nitrogen and heme iron in CYP11B1, as well as in reducing the adrenocortical suppression. Based on the results of ADMET property prediction, MEP analysis, and molecular docking simulation, 4-fluoroetomidate (EL-0052) was designed and synthesized. *In vivo* studies in rats and mice confirmed that EL-0052 had the efficacy similar to etomidate, but without adrenocortical suppression. These findings suggested that EL-0052 was superior to etomidate and support the continued development of EL-0052 as a preclinical candidate as an anesthetic.

© 2021 The Author(s). Published by Elsevier B.V. on behalf of Research Network of Computational and Structural Biotechnology. This is an open access article under the CC BY-NC-ND license (<http://creativecommons.org/licenses/by-nc-nd/4.0/>).

## 1. Introduction

Etomidate, the ethyl ester of 1-( $\alpha$ -methylbenzyl) imidazole-5-carboxylic acid, is a substituted imidazole that is used in the form of its active D-isomer. It can inhibit the excitability of CNS function by modulating multiple modes of  $\gamma$ -aminobutyric acid A receptor (GABA<sub>A</sub>R) mediated inhibition [1]. Because of its rapid onset of action, quick recovery from anesthetic effects, a wide therapeutic index (TI), a short context-sensitive half-life, and favorable hemodynamic stability [2,3], it has long been used for brief, deep sedation and induction of general anesthesia since 1972 [4]. Unfortunately, etomidate has been reported to inhibit the cytochrome P450 enzyme, 11 $\beta$ -hydroxylase 1 (CYP11B1), at hypnotic doses, thereby suppressing the biosynthesis of cortisol and preventing the adrenocortical stress response [5,6]. This side effect of primary hypoadrenocorticism persists long after the hypnotic effects of the drug have dissipated and is associated with a marked increase in patient deaths due to this unexpected off-target effect

[7,8]. This potential serious consequence of sustained adrenocortical suppression precludes the use of etomidate in maintaining anesthesia through continuous infusion and has aroused serious concerns regarding the administration of even a single bolus dose for the induction of anesthesia in critically ill patients [9–11].

Etomidate fulfills several characteristics of an ideal anesthetic agent, such as rapid onset with rapid clearance and high potency, along with cardiovascular stability. Reducing or eliminating the risk of adrenocortical suppression may provide an ideal anesthetic agent for prolonged infusions. Pharmacologists and medicinal chemists have attempted to develop numerous etomidate derivatives (Fig. 1) that retain the desirable properties of etomidate without the undesirable effect of adrenocortical insufficiency [12]. It has been established that adrenocortical suppression is mediated through the binding of the nitrogen of the etomidate imidazole ring with the 11 $\beta$ -hydroxylase. Carboetomidate is obtained by replacing the nitrogen of etomidate with a methylene group. Compared to etomidate, carboetomidate has a significantly lower inhibitory effect on cortisol synthesis; however, its anesthetic activity is only half as much as that of etomidate [13–15]. Based on the soft drug approach, methoxycarbonyl-etomidate (MOC-ET) with a rapid and predictable metabolic breakdown has been designed,

\* Corresponding authors.

E-mail addresses: [orangedp@cqmu.edu.cn](mailto:orangedp@cqmu.edu.cn) (P. Deng), [liqingeng@cqmu.edu.cn](mailto:liqingeng@cqmu.edu.cn) (Q.-g. Li).

<sup>1</sup> These authors contributed equally to this work

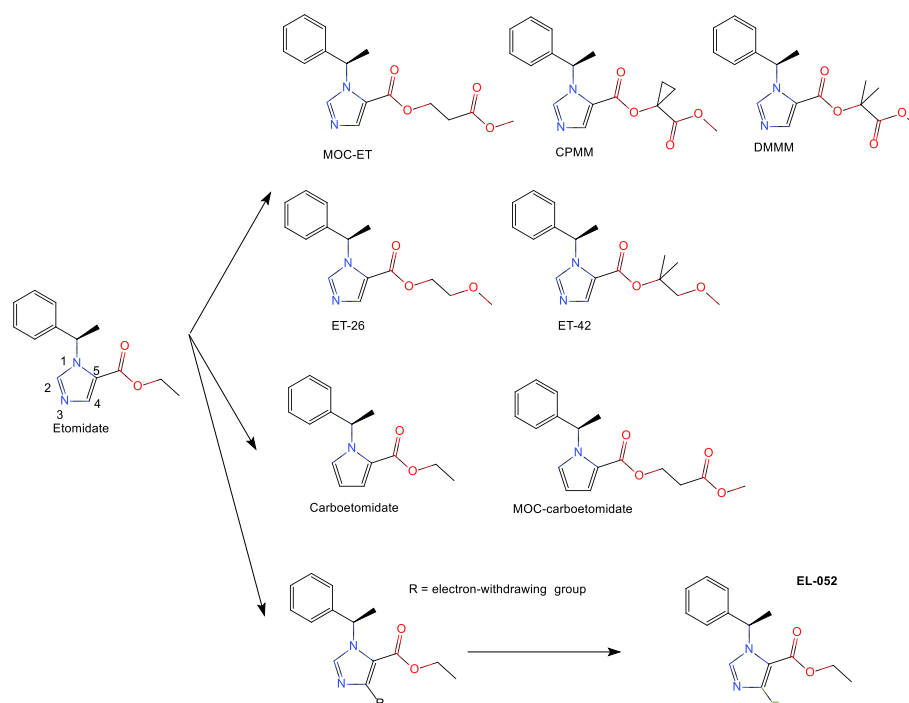


Fig. 1. Structure of etomidate and its derivatives.

which does not affect corticosterone synthesis following a single intravenous dose [16,17]. To improve the pharmacokinetics of MOC-ET, cyclopropyl-methoxycarbonyl metomidate (CPMM), and dimethyl-methoxycarbonyl metomidate (DMMM), methoxyethyl etomidate (ET-26), and methoxy-2-methylpropan etomidate (ET-42) have been designed [18–21]. With an aim of combining the favorable effects of both MOC-ET and carboetomidate, methoxycarbonyl-carboetomidate (MOC-carboetomidate), which is more rapidly metabolized and exhibits about half the activity than that of carboetomidate, has been designed [22]. Unfortunately, the 50% effective doses ( $ED_{50}$ ) of CPMM, ET-42, ET-26, and MOC-ET required to induce anesthesia intravenously in Beagle dogs are 0.59, 0.72, 1.44, and 23.12 mg/kg, respectively. These  $ED_{50}$ s are higher than that of etomidate (0.43 mg/kg) [21]. Carboetomidate and MOC-etomidate represent the successful pharmacodynamic and pharmacokinetic solutions to the problem of etomidate-induced adrenocortical suppression, respectively. Notably, the risk of adrenocortical suppression of these derivatives is significantly reduced. Unfortunately, the reduction in adrenocortical suppression is at the expense of compromising anesthetic potency. Therefore, these drugs may be not suitable for clinical development owing to their inherent pharmacological properties.

With the great progress in the study of the mechanism of action of general anesthetics, new structure, such as ciprofol (WO2015CN88341 20150828), or new formulation, such as the aqueous formulation of alphaxalone, have been developed [23–24]. However, little progress has been achieved over the past decades in developing safer anesthetic agents based on etomidate [25]. With the rapid development of computer software and hardware technology, computational approaches are supposed to streamline the drug discovery process in a manner that has great potential to develop anesthetic drugs [26–28]. Since the exact molecular structure of the heteropentameric  $GABA_A$ R remained unknown, a homology model of the  $GABA_A$ R was constructed using the homologous glycine and glutamate-gated chloride receptors as templates by computational approaches in 2018 [29]. Through in silico screening using this homology model, a class of N-

arylpyrrole derivatives were identified in 2019 [30]. Recently, several important CryoEM structures of human  $\alpha 1\beta 3\gamma 2$   $GABA_A$ R in complex with ligands (PDB IDs: 6HUP, 6HUO, 6HUK, 6HUJ, and 6HUG) [31] and the X-RAY structure of human CYP11B1 (PDB ID: 6M7X) [32] have been released. Thus, these new structures could provide even more accurate predictions of anesthetic activity and adrenocortical suppression.

To improve the parent drug, etomidate derivatives with an electron-withdrawing group in the imidazole ring were designed using computational approaches and synthesized in this study to reduce the coordination bond between the imidazole nitrogen and heme iron in CYP11B1.

## 2. Materials and methods

### 2.1. Molecular docking

CryoEM structure of human  $\alpha 1\beta 3\gamma 2$   $GABA_A$ R in complex with diazepam (PDB ID: 6HUP) and picrotoxin (PDB ID: 6HUJ) were first reported in 2019 [31]. Recent studies have shown that diazepam binds to the transmembrane receptor binding site of etomidate and is proved to be a competitive antagonist of etomidate [33]. Therefore, the structure (PDB ID: 6HUP) with diazepam binding to the site in the interfaces of  $\beta 3^+/\alpha 1^-$  transmembrane domain (TMD) suggests that the  $\alpha 1\beta 3\gamma 2$   $GABA_A$ R is in a desensitized conformation with anesthetics. Picrotoxin can reduce the apparent agonist affinity and increase the dissociation of GABA; thus the picrotoxin-bound structure (PDB ID: 6HUJ) is supposed to illustrate the  $\alpha 1\beta 3\gamma 2$   $GABA_A$ R in a closed/resting state. The binding modes of diazepam and picrotoxin were in agreement with the results of cysteine crosslinking experiments. 6HUP and 6HUJ represent the desensitized state and closed/resting states of the human  $\alpha 1\beta 3\gamma 2$   $GABA_A$ R, respectively. Moreover, diazepam and picrotoxin bound in the pocket formed by amino acids including  $\alpha 1M236$ ,  $\beta 3M286$ , and  $\beta 3N265$ , while those amino acids have been confirmed to interact with etomidate by experimental methods [34–35].

Besides, diazepam, picrotoxin, and etomidate have similar molecular sizes, so 6HUP was used as a docking target. To ensure the feasibility of the results, molecular dynamics simulation was further used to simulate this binding mode.

The structures of GABA<sub>A</sub>R (PDB IDs: 6HUP and 6HUJ) and CYP11B1 (PDB ID: 6M7X) were obtained in the Protein Data Bank (PDB; [www.rcsb.org](http://www.rcsb.org)) [36]. The Prepare Protein protocol in Discovery Studio 2017R2 (DS) software ([www.3dsbiovia.com](http://www.3dsbiovia.com)) was used for preparing the protein structures. Tasks, such as inserting missing atoms in incomplete residues, modeling the missing loop regions, deleting alternate conformations (disorder), removing water molecules, standardizing atom names, and protonating the titratable residues using predicted pKs, were executed.

The starting conformations of ligands were constructed using the GaussView 5.0 program. All ligands were optimized using the Gaussian 09 program ([www.gaussian.com](http://www.gaussian.com)) and the density functional theory (DFT) method at the B3LYP/6-311G (d, p) level. To simulate real conditions, the solvent effects of H<sub>2</sub>O were studied using the polarized continuum model (PCM).

To validate docking reliability, CDOCKER [37] and LibDock [38] protocol in DS were both used to re-dock ligands to the active sites, parameters are shown in Table 1S and 2S. The docking results with a root mean square deviation (RMSD) of heavy atoms <2.0 Å indicates that the docking method is feasible and the docking results is credible. For GABA<sub>A</sub>R, both CDOCKER and LibDock can reproduce the diazepam conformation in the crystal structure, and CDOCKER (RMSD: 0.43 Å) can get better results (Fig. 1S) than LibDock (RMSD: 0.92 Å). Therefore, CDOCKER was selected to simulate the docking of GABA<sub>A</sub>R. For CYP11B1, CDOCKER can not reproduce the conformation of fadrozole in the crystal structure (RMSD > 2.0 Å), while LibDock can get good results (RMSD: 0.32 Å). Therefore, LibDock was selected to simulate the docking of CYP11B1. Because molecular docking can not simulate the most important coordination bond interaction between CYP11B1 and etomidate, the Minimization (QM/MM) protocol in DS was used to optimize the docking results to obtain more accurate conformation.

To compare the affinity, the binding energies between the docking conformation and GABA<sub>A</sub>R were estimated using the poisson boltzmann with non-polar surface area (PBSA) solvent model in the Calculate Binding Energies protocol, parameters are shown in Table 3S. The binding energy was calculated using the following equation:

$$E_{\text{Binding}} = E_{\text{Complex}} - E_{\text{Ligand}} - E_{\text{Receptor}}$$

For transmembrane binding sites, the membrane model can better simulate the real conditions. Due to the limitation of this software, the effect of membrane was not considered in this study.

## 2.2. Docking poses minimization (QM/MM)

To get more accurate conformations, the QM/MM protocol in DS was used to minimize the energy of the structures through geometry optimization using the hybrid delocalized internal coordinate (HDLC) optimizer [39]. The QM region of atoms was treated with a quantum calculation using the DMol3 server with PBE function and the rest, MM region, was handled using the CHARMM forcefield [40]. The QM region of the QM/MM hybrid mechanics was used for the ligand and selected residues from the binding pocket surrounding the ligand (12 residues were considered for the GABA<sub>A</sub>R: L232, P233, M236, T237, L240, and L269 on the α1 subunit, and V258, N265, M286, F289, and V290 on the β3 subunit; the protoporphyrin IX containing Fe and C450 were considered for CYP11B1). As the B3LYP function may give better results but requires significantly more CPU time, the pose with the lowest QUANTUM energy was re-minimized using the QM/MM method with B3LYP function to obtain more accurate conformations. The

final pose minimized using the B3LYP function was used to analyze the binding model. The QM/MM results showed that the conformations of diazepam and fadrozole obtained using QM/MM minimization were highly consistent with that of the crystal. RMSD of heavy atoms were 0.33 Å and 0.26 Å respectively, indicating that the docking method was feasible and the QM/MM results were credible.

## 2.3. Pharmacokinetic (PK) parameters and prediction of physicochemical properties

The PK parameters, such as absorption, distribution, metabolism, excretion, and toxicity (ADMET), are important aspects in anesthetic drug discovery. In silico ADMET descriptors may provide useful information to predict the drug-likeness and druggability of lead compounds. To evaluate these properties of the selected hits, the molecular, physicochemical, and PK parameters were predicted using pkCSM [41] and the PK properties of EL-0052 and etomidate were compared.

Based on the electronic wavefunction provided by Gaussian 09, the surface electrostatic potential distribution and its extreme point were obtained using the wave function analysis software, Multiwfn (<http://sobereva.com/wfnbbs>) [42] and visualized using the VMD program (<https://www.ks.uiuc.edu/Research/vmd/>) [43].

## 2.4. Synthesis

A mixture of 1H-4-fluoroimidazole-5-carboxylate (134 mg, 1.1 mmol) and Ph<sub>3</sub>P (340 mg, 1.3 mmol) in dry THF (3 mL) was added dropwise to S-phenylethanol (134 mg, 1.1 mmol) in dry THF (2 mL). Then, DEAD (230 mg, 1.32 mmol) in dry THF (2 mL) was added dropwise to the reaction solution and the temperature was slowly raised to 0 °C. The reaction was monitored using TLC. After the reaction was complete, the solvent was removed by evaporation under reduced pressure. The residue was separated using column chromatography (EA:PA = 1:3) to obtain EL-0052. The synthesis and biological experimental methods are described in detail in the patent documents (PCT/CN2016/10696, 201680059075.4, US10392352, EP16853130.9, CN201680059075.4, CA3001431, and JP2018-537709), and these data are publicly available.

## 2.5. Biological and animal experiment

All animal experiments were conducted in accordance with the Guide for Care and Use of Laboratory Animals (8th edition) and approved by Institutional Animal Care and Use Committee (IACUC) in Jiangsu Nhwa Pharmaceutical Corporation Ltd. (Xuzhou, China). SD rats and mice were purchased from Shanghai SIPPR-Bk Lab Animal Co., Ltd.

EI-0052 (5 mg) was accurately weighed and transferred to a 10 mL centrifuge tube and 1 mL blank emulsion (20% soybean oil blank emulsion) was added. The mixture was sonicated in an ultrasonic apparatus for several minutes to obtain a 5 mg/mL homogeneous emulsion, which was drawn using an injection syringe right before use. Etomidate fat emulsion injection (2 mg/mL) was used as a control group. The ED<sub>50</sub> and median lethal dose (LD<sub>50</sub>) were measured before and after anesthesia using the sequential method. The preliminary experiment determined the approximate dose leading to anesthesia (or death) in mice, which was then chosen as the intermediate dosage in the actual experiments. Two to three dosage groups were set above and below the intermediate dosage group with an interval of 0.8. The disappearance of righting reflex or death was used as indicators of anesthetic efficacy or the toxicity index (TI) of drugs. The formal trial was started with the admin-

istration of the intermediate dose. If mice were anesthetized, a lower dosage was administered; otherwise a higher dose is given.

LD<sub>50</sub> and ED<sub>50</sub> values of anesthesia were calculated using a sequential method on aot425 software and the TI was calculated using the formula,  $TI = LD_{50}/ED_{50}$ .

Ten male mice were divided into two groups with five per group. The test drug was injected into the tail vein at a constant rate and the process was completed in 10 s. The disappearance time (latency) and recovery time (duration) of the righting reflex were recorded.

Male SD rats were divided into three groups after carotid intubation as follows: negative control group (n = 5), etomidate group (n = 8), EL-0052 group (n = 8). The animals were administered 0.2 mg/kg dexamethasone using tail vein injection. After 2 h, the baseline values of serum corticosterone were measured by carotid catheterization (C<sub>0min</sub> of corticosterone). Then, 0.2 mg/kg dexamethasone, EL-0052, and etomidate (positive control) were administered to the animals in the groups, respectively. Next, 25 µg/kg ACTH1-24 was immediately injected into the tail vein to stimulate corticosterone secretion. After 15 min, blood was collected through carotid catheterization and the concentration of corticosterone (C<sub>15min</sub> of corticosterone) was measured.

### 3. Results

#### 3.1. Structural insights into GABA<sub>A</sub>R and binding model analyses

GABA<sub>A</sub>R are ligand-gated chloride channels with many modulators, such as benzodiazepines and general anesthetics. Among the numerous assemblies that are theoretically possible, the  $\alpha 1\beta 2\gamma 2$  GABA<sub>A</sub>R is one of the two most prevalent isoforms in the brain. Several cryo-electron microscopy structures of  $\alpha 1\beta 3\gamma 2$  GABA<sub>A</sub>R bound to the agonist GABA, the classical benzodiazepines diazepam (PDB ID: 6HUP) and alprazolam (PDB ID: 6HUO), the channel-blocker picrotoxin (PDB IDs: 6HUJ and 6HUG), and the competitive antagonist bicuculline (PDB ID: 6HUK), are reported in the Protein Data Bank (PDB; www.rcsb.org). 6HUJ is supposed to illustrate the  $\alpha 1\beta 3\gamma 2$  GABA<sub>A</sub>R in a closed/resting state. 6HUP suggests that the  $\alpha 1\beta 3\gamma 2$  GABA<sub>A</sub>R is in a desensitized conformation with anesthetics.

Superposition of 6HUP (red/blue) and 6HUJ (grey) based on the global alignment was used to analyze the structural differences on the TMD (Fig. 2A). Differences in the relative orientations of the TMD between the desensitized and closed/resting states illustrate how anesthetics induced the translation motion of  $\alpha 1$  and  $\beta 3$  subunits on the TMD. Notably, the binding of anesthetics results in the translation motion of  $\alpha 1$  and  $\beta 3$  subunits in the opposite direction, which increases the gap between  $\alpha 1$  and  $\beta 3$  subunits (Fig. 2B), and then leads to the opening of the chloride channels.

As shown in Fig. 3 and Fig. 2S, in the binding pocket, the phenyl ring shows hydrophobic interactions with  $\beta 3M286$  and  $\alpha 1P233$ , and points towards  $\alpha 1L232$  located at the pocket opening; the imidazole ring in involved in hydrophobic interactions with  $\alpha 1L269$  and  $\alpha 1P233$ , while the H atom belonging to C2-H bond points towards  $\beta 3N265$ ; the methyl is involved in hydrophobic interactions with  $\beta 3F289$ , while the ethyl group forms hydrophobic interactions with  $\beta 3V258$  and  $\alpha 1L240$ ; a pi-sulfur interaction can be observed between  $\alpha 1M236$  and the phenyl ring (Fig. 3B). Notably, a weak non-classical hydrogen bond between an H atom in ethyl and  $\alpha 1T237$  with a bond length of 2.48 Å is formed. Another non-classical hydrogen bond between the donor (C2-H in imidazole ring) and the acceptor (carbonyl of  $\beta 3N265$ ) with a bond length of 2.12 Å is formed, which cannot be formed between carboetomidate and  $\beta 3N265$ . The substitution of nitrogen with the methylene group reduces the positive electrostatic potential of

the H atom in the C2-H bond in carboetomidate, which is not conducive to the formation of the hydrogen bond. This may explain why the anesthetic activity of carboetomidate is significantly reduced.

Molecular recognition events between anesthetics and receptors are mainly driven by non covalent interactions. In etomidate, the strong electron withdrawing carbonyl group is directly connected with the imidazole, which makes the H atom on the imidazole in the electron deficient state and easy to form non-classical hydrogen bonds with the electron donating group of the acceptor amino acid.

#### 3.2. Structural insights into CYP11B1 and binding mode analyses

Based on the CYP11B1 homology models, the binding between etomidate and CYP11B1 has been predicted using the docking method in 2013 [13]. Molecular modeling results predicted that etomidate may bind with the heme iron involving the carbonyl oxygen or the imidazole nitrogen. However, the further photolabeling and spectroscopy indicate that the putative carbonyl-iron interaction is insufficient to stabilize the binding of carboetomidate to CYP11B1<sup>13</sup>. To verify its accuracy, the X-ray structure of human CYP11B1 (PDB ID: 6M7X) was used for molecular docking with etomidate in this study. The docking results are consistent with those of previous studies and provide a more detailed interaction.

The binding site formed by the porphyrin-iron and hydrophobic amino acids is located in the center of CYP11B1 (Fig. 4A). Our docking studies revealed that etomidate binds in the CYP11B1 active site with a nitrogen atom of the imidazole ring coordinated vertically to the iron atom of the porphyrin ring, with a bond length about 1.96 Å (Fig. 4B). Thus, the imidazole ring oriented almost perpendicularly to the heme plane, which is conducive to the formation of stable coordination bonds. The residues around the active site may increase the affinity of etomidate and CYP11B1 through the hydrophobic interactions and non-classical hydrogen bonds (Fig. 4B).

#### 3.3. Design of etomidate derivative and its predicted ADMET and physicochemical properties

The substitution on the nitrogen atom of the imidazole ring by methylene not only significantly reduce adrenocortical suppression but also greatly reduces the anesthetic efficiency of etomidate. It indicates that the nitrogen atom in the imidazole ring has a specific contribution to the binding of etomidate to GABA<sub>A</sub>R and CYP11B1. It seems necessary to retain the N3 atom in the imidazole ring. Based on the analysis of binding mode, we presume that the strong electron-withdrawing groups on the imidazole ring tend to reduce the charge density of the nitrogen, which may be beneficial in reducing the coordination bond between the imidazole nitrogen and heme iron in CYP11B1, thereby reducing adrenocortical suppression. Therefore, 4-fluoroetomidate (EL-0052) was designed (Fig. 5).

Satisfactory ADMET properties may improve the success rate of drug design. The pharmacokinetic properties predicted using in silico screening approaches are listed in Table 1. Owing to the high structural similarity, ADMET properties of the designed derivatives are almost the same as those of etomidate, which indicates that EL-0052 may have similar pharmacokinetic properties.

The molecular electrostatic potential (MEP) at a point is defined as the energy required to bring a single positive charge from infinity to that point. Since MEP plays a crucial role in determining the electrostatically dominated weak interaction between a system and other substances, the calculation of the MEP was suggested as a practical and rapid method to estimate the coordination trend

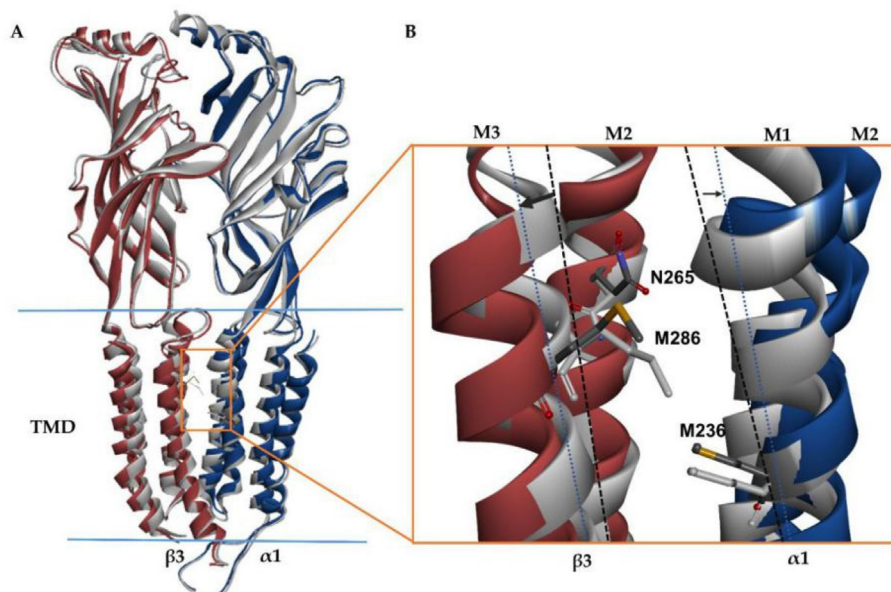


**Fig. 2.** (A) The  $\beta 3^*/\alpha 1^-$  TMD interface conformational differences between the desensitized (PDB ID: 6HUP) and closed/resting conformation (PDB ID: 6HUJ) of GABA<sub>A</sub>R based on the global alignment. The closed/resting conformation is shown in grey and the desensitized conformation is colored by subunit ( $\alpha 1$ , blue;  $\beta 3$ , red). The binding sites of general anesthetics are located at the upper-middle part of the  $\beta 3^*/\alpha 1^-$  TMD interfaces, which are displayed in the orange frame. (B) Schematic illustration of TMD conformational changes initiated by binding of the anesthetics. Binding of anesthetics results in the translation motion of  $\alpha 1$  and  $\beta 3$  subunits in the opposite directions; the black arrows indicate the direction of translation motion, with increasing arrow thickness representing a greater magnitude of translation motion. Oblique dotted lines indicate the putative position of the skeleton of the  $\alpha$ -helix M3 in  $\alpha 1$  subunit and  $\alpha$ -helix M1 in  $\beta 3$  subunit, respectively (blue represents desensitized conformation; black represents the closed/resting conformation).  $\alpha 1$ M236,  $\beta 3$ M286, and  $\beta 3$ N265 confirmed to interact with etomidate using experimental approaches are displayed in the stick model. (For interpretation of the references to color in this figure legend, the reader is referred to the web version of this article.)

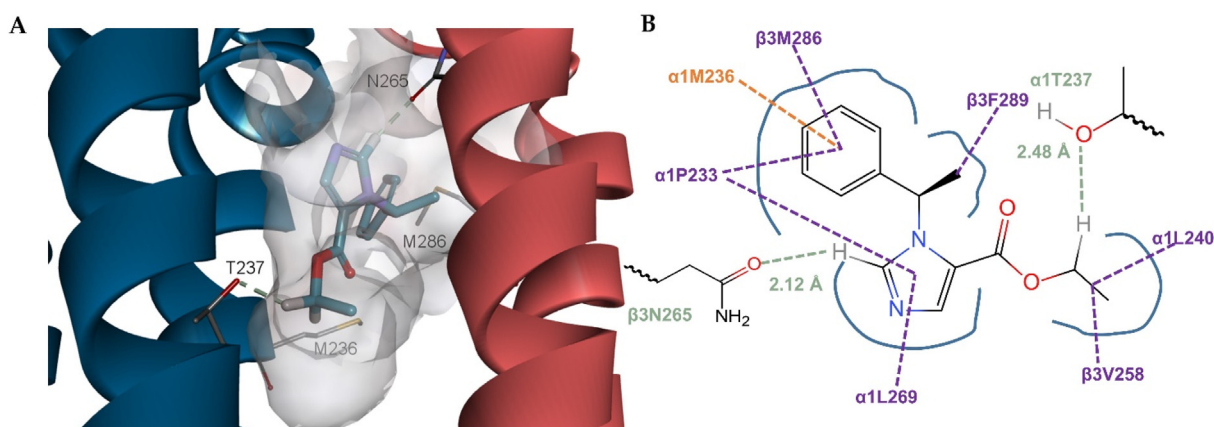


**Fig. 3.** (A) 3D diagram of the interaction between etomidate and GABA<sub>A</sub>R. (B) the etomidate-receptor interactions are shown as a 2D diagram. Hydrophobic interactions are represented by purple bonds, non-classical hydrogen bonds by light green bonds, and pi-sulfur interactions by the yellow bond, dark blue curved lines represent the frontiers of amino acid residues binding to etomidate. (For interpretation of the references to color in this figure legend, the reader is referred to the web version of this article.)

intuitively. The isosurface of MEP for etomidate and EL-0052 under a properly selected isovalue were calculated and plotted (Fig. 6). The MEP in the nitrogen region of the imidazole ring in the etomidate is negative, enabling it to form a coordination bond with the heme iron in CYP11B1. With the introduction of an F atom, the minima of MEP above the nitrogen atom region of the imidazole ring increased from  $-47.04$  kcal/mol to  $-43.93$  kcal/mol, indicating that the ability of imidazole to form a coordination bond with iron decreases gradually. In the binding mode analysis, it was found that the non-classical hydrogen bond between the H atom of C2-H bond in the imidazole ring and  $\beta 3$ N265 was formed. The maxima of MEP above this Hydrogen region of the imidazole ring increased from 28.8 kcal/mol (etomidate) to 34.29 kcal/mol (EL-0052), indicating that the introduction of halogen atom was con-

ductive to strengthening this hydrogen bond. In conclusion, EL-0052 may be a potential anesthetic because the F atom has great electron absorption ability and can significantly improve the MEP values above the N3 atom and the H atom belonging to the C2-H bond in the imidazole ring.

#### 3.4. Hit compound

The calculated results showed that the predicted ADMET properties of EL-0052 were similar to those of etomidate. The MEP indicated that halogen substitution could reduce the coordination effect of etomidate and CYP11B1 and increase the interaction between etomidate and GABA<sub>A</sub>R, which may be an effective way to modify the structure of etomidate. Furthermore, the molecular

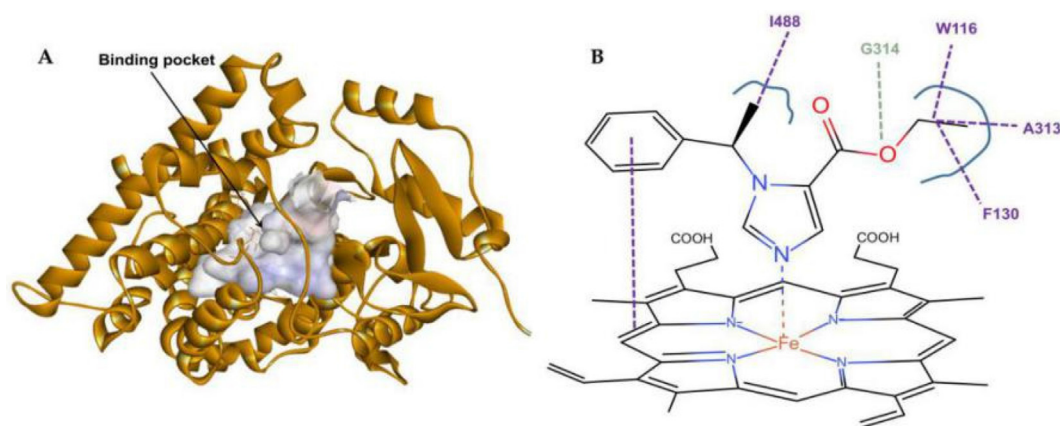


**Fig. 4.** (A) Structure of human CYP11B1 in complex with etomidate. (B) Etomidate-CYP11B1 interactions. Hydrophobic interactions are represented by purple bonds, non-classical hydrogen bonds by light green bond, and dark blue curved lines represent the frontiers of amino acid residues binding to etomidate. (For interpretation of the references to color in this figure legend, the reader is referred to the web version of this article.)

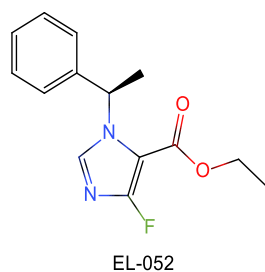


**Fig. 5.** Structures of the fluorinated derivative of etomidate (EL-00052).

docking method was used to predict the mode of action of EL-0052 and GABA<sub>A</sub>R. Fortunately, docking results show that EL-0052 and etomidate have the same binding mode (Fig. 7). Based on the above study, EL-0052 was synthesized and its anesthetic activity was verified.

### 3.5. Chemistry

EL-00052 (81 mg) was synthesized using a dehydration reaction between 1H and 4-fluoroimidazole-5-carboxylate (134 mg, 1.1 mmol) and S-phenylethanol (134 mg, 1.1 mmol) with a yield of 28% (Scheme 1).

$ESI[M + H]^+ = 263.24$ .

<sup>1</sup>H NMR (CD<sub>3</sub>Cl, 400MHz) 1.31 (t, *j* = 7.1 Hz, 3H); 1.96 (d, *j* = 7.2 Hz, 3H); 4.20–4.33 (q, *j* = 7.1 Hz, 2H); 6.22–6.31 (m, 1H), 7.16–7.38 (m, 5H).

F-NMR δ: −113.40 (s).

### 3.6. Biological evaluation

EL-0052 shows an anesthetic efficacy in mice (ED<sub>50</sub> ≈ 2.0 mg/kg), which is close to that of etomidate (Table 2), with a rapid onset and a short duration of action (Table 3).

**Table 1**

ADMET properties. tPSA, Topological molecular polar surface area; WS, Water solubility; P-gp, P-glycoprotein substrate; log BB, BBB permeability; log PS, CNS permeability; CYP2D6, CYP2D6 substrate; CYP3A4, CYP3A4 substrate; ClTot, Total Clearance; hERG, ERG inhibitor.

	cLogP	tPSA	WS	P-gp	logBB	logPS	CYP2D6	CYP3A4	ClTot	hERG
EL-0052	2.253	44.12	−2.318	YES	0.637	−1.750	No	No	1.141	No
Etomidate	2.114	44.12	−2.231	YES	0.439	−1.747	No	No	1.296	No
Propofol	3.639	20.23	−4.014	NO	0.664	−1.361	No	No	0.206	No
Diazepam	3.154	32.67	−4.444	YES	0.334	−1.350	No	YES	0.297	No

The results from statistical analyses (Table 4) showed that the concentration of corticosterone (C<sub>15min</sub>) in the etomidate group (positive control) was significantly lower than that in the negative control group (*P* < 0.05), indicating that etomidate had an inhibitory effect on cortisol biosynthesis. The concentration of corticosterone (C<sub>15min</sub>) in the EL-0052 group was significantly higher than that of etomidate (*P* < 0.001) and the control group (*P* < 0.05), indicating that EL-0052 did not inhibit the synthesis of cortisol.

These findings confirmed that EL-0052 was superior to etomidate, thereby supporting the continued development of EL-0052 as a preclinical candidate compound.

## 4. Discussion

The molecular target, GABA<sub>A</sub>R, is a validated and attractive drug design protein for the development of anesthetics. In addition, CYP11B1 is also recognized as an alternative target related to the off-target activity of etomidate. The CryoEM structure of human α1β3γ2 GABA<sub>A</sub>R and the X-RAY structure of human CYP11B1 have both been made available. Molecular docking can well simulate the interaction between a drug and its target [44]. These new structures can provide more accurate information for the structure-based computer-aided design of anesthetics.

The predicted binding modes of the top five for etomidate with GABA<sub>A</sub>R are shown in Fig. 2S–6S. In order to select a reasonable combination model, the binding energies were evaluated. Binding mode 1 (Figs. 3 and 2S) appears the most plausible. (1) Binding mode 1 is in agreement with the results of the photo-affinity labeling experiments, in which the residue α1M236 of α-helix M1 and residues β3M286 and β3N265 of α-helix M3 are identified as the determinant of etomidate sensitivity [33]. The high-affinity sites for etomidate have been found at the subunit interfaces of β3\*/α1<sup>−</sup> TMD [34]. The interaction between etomidate and the above amino acid residues is well demonstrated in model 1. Besides, eto-

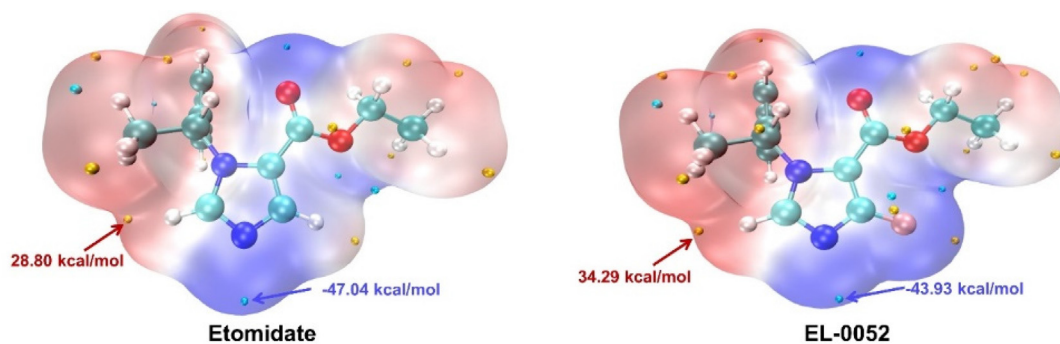


**Fig. 6.** Molecular electrostatic potential (MEP) mapped van der Waals surface (0.001 a.u. isosurface) of etomidate and EL-0052. The redder the color, the more positive the ESP. Minima and maxima of MEP on the surface are drawn as cyan and orange spheres, respectively. (For interpretation of the references to color in this figure legend, the reader is referred to the web version of this article.)

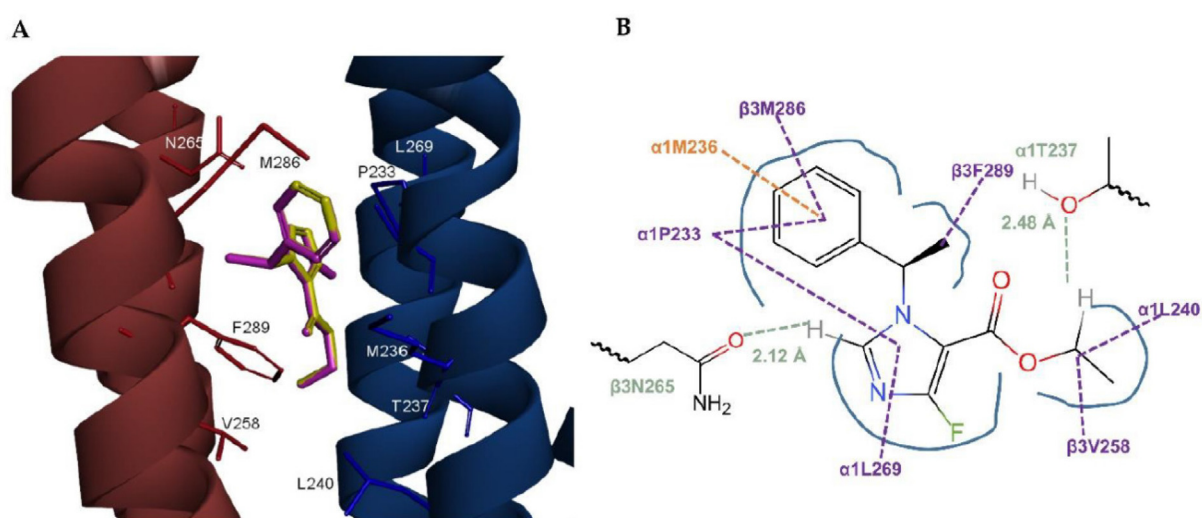
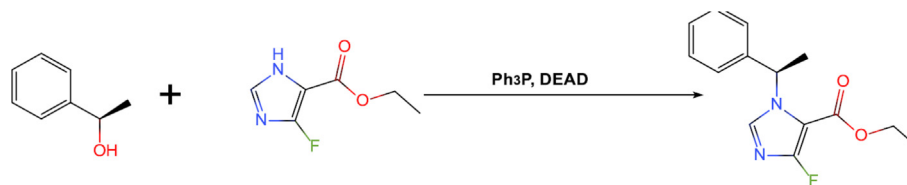


**Fig. 7.** (A) The binding mode of etomidate (yellow sticks) and EL-00052 (purple sticks). Molecules were docked in the DZP binding site (PDB ID: 6HUP). (B) EL-0052-receptor interactions are shown as a 2D diagram. Hydrophobic interactions are represented by purple bonds, non-classical hydrogen bonds by light green bonds, and the pi-sulfur interaction by a yellow bond; dark blue curved lines represent the frontiers of amino acid residues binding to etomidate. (For interpretation of the references to color in this figure legend, the reader is referred to the web version of this article.)



**Scheme 1.** Synthesis of EL-00052.

**Table 2**

LD<sub>50</sub>, ED<sub>50</sub>, and therapeutic index (TI) of EL-0052 and etomidate in mice (n = 10–20).

	LD <sub>50</sub> (mg/kg)	ED <sub>50</sub> (mg/kg)	TI*
Etomidate	50.3 (46.6–55.8)	2.0 (1.8–2.3)	25.1
EL-0052	46.5 (42.7–50.7)	2.0 (1.8–2.3)	23.3

The data in brackets represent 95% confidence intervals.

\* TI index = LD<sub>50</sub>/ED<sub>50</sub>.

**Table 3**

Latent and persistent periods of anesthesia of EL-0052 and etomidate in mice (mg/kg, n = 5).

	Dosage (mg/kg)	Latent period (s)	Persistent period (s)
Etomidate	6 (3*ED <sub>50</sub> )	5.4 ± 0.5	175.5 ± 100.1
EL-0052	6 (3*ED <sub>50</sub> )	5.8 ± 0.8	82.1 ± 20.2

midate binds to GABA<sub>A</sub>R by hydrogen bonding and hydrophobic interactions with the amino acid residues around the active site (Fig. 3B). (2) The conformation of the ester bond toward the cavity formed by the two subunits is reasonable. This can explain why

MOC-ET, CPMM, ET-42, and ET-26 with long side chains still have anesthetic activity. (iii) The binding mode 1 results in a reasonable PBSA binding energy. As a control computational experiment, the role of the non-classical hydrogen bond was further investigated in new docking experiments using a triazole derivative (Fig. 7S).

**Table 4**  
Effects of EL-0052 and etomidate on corticosterone secretion in rats.

	Dosage (mg/kg)	C <sub>0min</sub>	C <sub>15min</sub>
Negative control (n = 5)	/	3.6 ± 0.7	60.0 ± 12.1
Etomidate (Positive control) (n = 8)	4	2.8 ± 0.4	19.5 ± 1.9*
EL-0052 (n = 8)	4	6.5 ± 3.7	88.8 ± 11.0 <sup>#</sup>

Compared with the negative control group, \* represents  $P < 0.05$ ; compared with the etomidate group, <sup>#</sup> represents  $P < 0.001$ .

A decrease in binding energy (Table 5S) indicate that the non-classical hydrogen bond between the H atom in the C2-H bond of the imidazole ring and  $\beta$ 3N265 plays an important role.

Relaxation of the proteins from their crystal-packed states was not evaluated using molecular dynamics in this study. Etomidate has a micromolar-range EC<sub>50</sub> with GABA<sub>A</sub>R, so it cannot be guaranteed to remain in the same bound configuration after such relaxation, or during thermal fluctuations. So the detailed interactions described might not be the correct ones.

In addition to the interaction between anesthetics and receptors, the pharmacokinetic properties of anesthetics are important, perhaps more important. Since the site of action is located in the transmembrane region, the favorability of these drugs partitioning into the lipid bilayer out of the aqueous phase and increasing the effective concentration at the effector site is also a key issue to be considered in the anesthetic design. The anesthetic efficiency of CPMM, ET-42, ET-26, and MOC-ET were significantly lower than that of etomidate, which may be related to the changes of their physicochemical properties, thus affecting their pharmacokinetic properties and decreasing the effective concentration of the effector site. A change in the ADMET properties caused by the substituents may further influence the anesthetic activity. Based on the above considerations, only one halogen atom was introduced in this design of etomidate derivatives, so that the new compounds can maintain the pharmacokinetic properties of etomidate to the greatest extent. From the theoretical prediction results (Table 1) and preliminary animal experimental data (Tables 2–4), the key pharmacokinetic properties of EL-0052 are close to etomidate.

Because of the non-classical hydrogen bond between the H atom in the C2-H bond of imidazole ring and  $\beta$ 3N265, the introduction of substituents on the C2 atom of imidazole may be detrimental to activity. In addition, the H atom belonging to the C2-H bond points towards the carbonyl group of  $\beta$ 3N265. Therefore, the repulsion between the electron-withdrawing substituents at the C2 position and carbonyl groups is not conducive to stable binding. Besides, the C4 atom of imidazole is close to the edge of the binding pocket; a large substituent group at the C4 atom introduces steric hindrance, which is detrimental to activity. In conclusion, in order not to change the binding mode of etomidate, only C4 substituents were designed. The substituents were limited to fluorine, without considering large electron-withdrawing groups, such as aldehyde, nitro, cyano, and trihalomethyl. Interestingly, fluorine is a very common group in anesthetics such as fluothane, methoxyflurane, enflurane, isoflurane, sevoflurane, desflurane, chloroform, ketamine, and benzodiazepines.

In the binding mode of etomidate and CYP11B1, the ethyl group on the ester bond is very close to the edge of the binding pocket; therefore, the introduction of large substituent groups may result in steric hindrance, which may destroy the coordination ability. This may be one of the reasons why ET-26 and ET-42 had no inhibition of the adrenocortical function. Reducing the coordination ability between the nitrogen atom and the heme plane and increasing the length of the side chains may be suitable approaches to reduce the side effects of etomidate.

Blood–brain barrier (BBB) and CNS permeability are the most important pharmacokinetic properties of anesthetics. Compounds with a logBB > 0.3 are considered to readily cross the BBB, and those with a log PS > -2 are considered to be capable of penetrating the central nervous system (CNS). Based on the predicted logBB and log PS values, EL-0052, etomidate, propofol, and diazepam all have a better ability to pass through the BBB and CNS, which is conducive to the production of central anesthesia. Both EL-0052 and etomidate are substrates of P-glycoprotein and have a similar total clearance rate, which means that EL-0052 may have similar advantages of the rapid onset of action and recovery from anesthetic effects as well as a short context-sensitive half-life.

The predicted ADMET properties and MEP calculations could likely support the findings discussed above.

Based on the in-depth analysis of the binding mode, EL-0052 was designed to reduce the coordination bond between imidazole nitrogen and heme iron in CYP11B1. *In vivo* studies in rats and mice have confirmed that EL-0052 has efficacy similar to etomidate, but without adrenocortical suppression.

Based on the good results of el-0052, it is worth trying to replace F with Cl, Br or I. Based on the active conformation of EL-0052 obtained by molecular docking, F was directly replaced by Cl, Br or I; and it can be seen that there is a steric hindrance between Cl, Br or I and the amino acid residue T265 due to the large volume of Cl, Br or I. Further docking results showed that the binding mode of these compounds was completely different from etomidate (Fig. 8S), which means that these compounds may have no activity. Unlike Cl, Br and I, the size of F atom is similar to that of H atom, so there is no extra steric hindrance. The docking results showed that the binding mode of EL-0052 with GABAAR was the same as that of etomidate (Fig. 7). Besides, the purpose of introducing halogen atoms is to reduce the charge density of N and weaken the coordination bond between N and iron. As we all know, ability of attract electron of Cl, Br and I are lower than F, so F is the best choice among halogen atoms. To verify the theoretical research conclusion, 4-chlorineetomidate, 4-bromineetomidate, 4-iodineetomidate were also synthesized and their anesthetic activities were tested. Unfortunately, the results showed that these compounds had no anesthetic activity.

## 5. Conclusion

EL-0052 was found to be superior to etomidate, which supports the continued development of EL-0052 as a preclinical candidate compound.

## Declaration of Competing Interests

X. Xu, T. Wang, L. Zeng, and Q. Li, are coinventors on several patent applications submitted by the Jiangsu Nhwa-Luokang Pharmaceutical Research and Development Corporation Ltd. They could receive royalties relating to the development of EL-0052.

## Acknowledgment

This study was supported by the Research Projects of Chongqing Medical University (NSFYY201824, ZHYX2019022).

## Appendix A. Supplementary data

Supplementary data to this article can be found online at <https://doi.org/10.1016/j.csbj.2021.01.002>.

## References

- [1] Herd MB, Lambert JJ, Belelli D. The general anaesthetic etomidate inhibits the excitability of mouse thalamocortical relay neurons by modulating multiple modes of GABA(A) receptor-mediated inhibition. *Eur J Neurosci* 2014;40:2487–501.
- [2] Morgan M, Lumley J, Whitwam JG. Respiratory effects of etomidate. *Brit J Anaesth* 1977;49:233–6.
- [3] Lee JM, Min G, Keum B, Lee JM, Kim SH, Choi HS, et al. Using Etomidate and midazolam for screening colonoscopies results in more stable hemodynamic responses in patients of all ages. *Gut Liver* 2019;13:649–57.
- [4] Rathore VS, Singh S, Taank P, Khandelwal A, Kaushal A. Clinical analysis of propofol, etomidate and an admixture of etomidate and propofol for induction of general anaesthesia. *Turkish J Anaesthesiol Reanim* 2019;47:382–6.
- [5] Alolio B, Stuttmann R, Leonhard U, Fischer H, Winkelmann W. Adrenocortical suppression by a single induction dose of etomidate. *Klin Wochenschr* 1984;62:1014–7.
- [6] de Jong FH, Mallios C, Jansen C, Scheck PA, Lamberts SW. Etomidate suppresses adrenocortical function by inhibition of 11 beta-hydroxylation. *J Clin Endocr Metab* 1984;59:1143–7.
- [7] Vinclair M, Broux C, Faure P, Brun J, Genty C, Jacquot C, et al. Duration of adrenal inhibition following a single dose of etomidate in critically ill patients. *Intens Care Med* 2008;34:714–9.
- [8] Watt I, Ledingham IM. Mortality amongst multiple trauma patients admitted to an intensive therapy unit. *Anaesthesia* 1984;39:973–81.
- [9] Komatsu R, You J, Mascha EJ, Sessler DI, Kasuya Y, Turan A. Anesthetic induction with etomidate, rather than propofol, is associated with increased 30-day mortality and cardiovascular morbidity after noncardiac surgery. *Anesth Analg* 2013;117:1329–37.
- [10] Chan CM, Mitchell AL, Shorr AF. Etomidate is associated with mortality and adrenal insufficiency in sepsis: A meta-analysis. *Crit Care Med* 2012;40:2945–53.
- [11] Gaessler M, Ruppert M, Lefering R, Bouillon B, Wafaisade A, TraumaRegister DGU. Pre-hospital emergent intubation in trauma patients: the influence of etomidate on mortality, morbidity and healthcare resource utilization. *Scand J Trauma Resusc Emerg Med* 2019;27:61.
- [12] Malapero RJ, Zaccagnino MP, Brovman EY, Kaye AD, Urman RD. Etomidate derivatives: Novel pharmaceutical agents in anesthesia. *J Anaesth Clin Pharmacol* 2017;33:429–31.
- [13] Shanmugasundararaj S, Zhou X, Neunzig J, Bernhardt R, Cotton JF, Ge R, et al. Carboetomidate: an analog of etomidate that interacts weakly with 11 beta-hydroxylase. *Anesth Analg* 2013;116:1249–56.
- [14] Cotton JF, Forman SA, Laha JK, Cuny GD, Husain S, Miller KW, et al. Carboetomidate a pyrrole analog of etomidate designed not to suppress adrenocortical function. *Anesthesiology* 2010;112:637–44.
- [15] Jackson WL. Carboetomidate: Will it eliminate the etomidate debate?. *Crit Care Med* 2012;40:333–4.
- [16] Cotton JF, Husain SS, Forman SA, Miller KW, Kelly EW, Nguyen HH, et al. Methoxycarbonyl-etomidate a novel rapidly metabolized and ultra-short-acting etomidate analogue that does not produce prolonged adrenocortical suppression. *Anesthesiology* 2009;111:240–9.
- [17] Ge RL, Pejo E, Haburcak M, Husain SS, Forman SA, Raines DE. Pharmacological studies of methoxycarbonyl etomidate's carboxylic acid metabolite. *Anesth Analg* 2012;115:305–8.
- [18] Valk BI, Absalom AR, Meyer P, Meier S, den Daas I, van Amsterdam K, et al. Safety and clinical effect of i.v. infusion of cyclopropyl-methoxycarbonyl etomidate (ABP-700), a soft analogue of etomidate, in healthy subjects. *Brit J Anaesth* 2018;120:1401–11.
- [19] Campagna JA, Pojasek K, Grayzel D, Randle J, Raines DE. Advancing novel anesthetics pharmacodynamic and pharmacokinetic studies of cyclopropyl-methoxycarbonyl metomidate in dogs. *Anesthesiology* 2014;121:1203–16.
- [20] Chitilian HV, Eckenhoff RG, Raines DE. Anesthetic drug development: Novel drugs and new approaches. *Surg Neurol Int* 2013;4(Suppl 1):S2–S10.
- [21] Yang J, Kang Y, Wang B, Yang L, Liu J, Zhang W. Metabolite-inactive etomidate analogues alleviating suppression on adrenal function in Beagle dogs. *Eur J Pharm Sci* 2017;99:343–9.
- [22] Pejo E, Cotton JF, Kelly EW, Ge RL, Cuny GD, Laha JK, et al. In vivo and in vitro pharmacological studies of methoxycarbonyl-carboetomidate. *Anesth Analg* 2012;115:297–304.
- [23] Monagle J, Siu L, Worrell J, Goodchild CS, Serrao JM. A phase 1c trial comparing the efficacy and safety of a new aqueous formulation of alphaxalone with propofol. *Anesth Analg* 2015;121:914–24.
- [24] Goodchild CS, Serrao JM, Kolosov A, Boyd BJ. Alphaxalone reformulated: a water-soluble intravenous anesthetic preparation in sulfobutyl-ether-beta-cyclodextrin. *Anesth Analg* 2015;120:1025–31.
- [25] Hemmings Jr HC, Riegelhaupt PM, Kelz MB, Solt K, Eckenhoff RG, Orser BA, et al. Towards a comprehensive understanding of anesthetic mechanisms of action: a decade of discovery. *Trends Pharmacol Sci* 2019;40:464–81.
- [26] McGrath M, Pence A, Raines DE. Computational approaches to anesthetic drug discovery. *Trends Pharmacol Sci* 2019;40:809–11.
- [27] Jiang JH, Deng P. Discovery of new inhibitors of transforming growth factor-beta type 1 receptor by utilizing docking and structure-activity relationship analysis. *Int J Mol Sci* 2019;20:4090.
- [28] Jiang JH, Zhou H, Jiang QH, Sun LL, Deng P. Novel transforming growth factor-beta receptor 1 antagonists through a pharmacophore-based virtual screening approach. *Molecules* 2018;23:2824.
- [29] Fahrenbach VS, Bertaccini EJ. Insights into receptor-based anesthetic pharmacophores and anesthetic-protein interactions. *Methods Enzymol* 2018;602:77–95.
- [30] Cayla NS, Dagne BA, Wu Y, Lu Y, Rodriguez L, Davies DL, et al. A newly developed anesthetic based on a unique chemical core. *Proc Natl Acad Sci USA* 2019;116(31):15706–15.
- [31] Masiulis S, Desai R, Uchanski T, Martin IS, Laverty D, Karia D, et al. GABA(A) receptor signalling mechanisms revealed by structural pharmacology. *Nature* 2019;565:454–9.
- [32] Brixius-Anderko S, Scott EE. Structure of human cortisol-producing cytochrome P450 11B1 bound to the breast cancer drug fadrozole provides insights for drug design. *J Biol Chem* 2019;294:453–60.
- [33] Li GD, Chiara DC, Sawyer GW, Husain SS, Olsen RW, Cohen JB. Identification of a gaba(a) receptor anesthetic binding site at subunit interfaces by photolabeling with an etomidate analog. *J Neurosci* 2006;26:11599–605.
- [34] McGrath M, Hoyt H, Pence A, Jayakar SS, Zhou XJ, Forman SA, et al. Competitive antagonism of etomidate action by diazepam in vitro GABA(A) receptor and in vivo zebrafish studies. *Anesthesiology* 2020;133:583–94.
- [35] Yip GMS, Chen ZW, Edge CJ, Smith EH, Dickinson R, Hohenester E, et al. A propofol binding site on mammalian GABA<sub>A</sub> receptors identified by photolabeling. *Nat Chem Biol* 2013;9:715–20.
- [36] Burley SK, Berman HM, Bhikadiya C, Bi C, Chen L, Di Costanzo L, et al. RCSB protein data bank: biological macromolecular structures enabling research and education in fundamental biology, biomedicine, biotechnology and energy. *Nucl Acids Res* 2019;47:D464–74.
- [37] Wu GS, Robertson DH, Brooks CL, Vieth M. Detailed analysis of grid-based molecular docking: A case study of CDOCKER - A CHARMM-based MD docking algorithm. *J Comput Chem* 2003;24:1549–62.
- [38] Diller DJ, Merz KM. High throughput docking for library design and library prioritization. *Proteins* 2001;43:113–24.
- [39] Billeter SR, Turner AJ, Thiel W. Linear scaling geometry optimisation and transition state search in hybrid delocalised internal coordinates. *Phys Chem Chem Phys* 2000;2:2177–86.
- [40] Momany FA, Rone RJ. Validation of the general purpose QUANTA 3.2/CHARMM force field. *Comp Chem* 1992;13:888–900.
- [41] Pires DEV, Blundell TL, Ascher DB. pkCSM: predicting small-molecule pharmacokinetic and toxicity properties using graph-based signatures. *J Med Chem* 2015;58:4066–72.
- [42] Lu T, Chen F. Multiwfn: A multifunctional wavefunction analyzer. *J Comput Chem* 2012;33:580–92.
- [43] Humphrey W, Dalke A, Schulten K. VMD: visual molecular dynamics. *J Mol Graph* 1996;14:33–8.
- [44] Wang S, Jiang JH, Li RY, Deng P. Docking-based virtual screening of TβR1 inhibitors: evaluation of pose prediction and scoring functions. *BMC Chem* 2020;14:52.